

Versatile Nicotinamide Enabling Dendrite-free and Efficient Deposition for Aqueous
Zn-I₂ Batteries

Hejing Wang^{1, #}, Yitian Su^{1, #}, Lijing Yan^{1, *}, Xiaomin Zeng^{2, *}, Xiaoran Chen¹, Baorui Xiang³,
Huixin Ren⁴, Tingli Ma¹, Min Ling^{2, *}

1. College of Materials and Chemistry, China Jiliang University, Hangzhou, 310018, China

2. College of Chemical and Biological Engineering, Zhejiang University, Hangzhou, 310027,
China

3. Department of Chemistry, Rice University, Houston, Texas 77005, United States

4. School of Chemical and Materials Engineering, Huizhou University, Huizhou, 516007,
China

Corresponding authors: yanlijing@cjlu.edu.cn; 11828027@zju.edu.cn; minling@zju.edu.cn

1. Material Preparation

The thickness of the zinc foil used in this work is 0.03 mm. NTA-0.1% (NTA-0.01%, NTA-1%): 0.1 wt% (0.01wt%, 1wt%) nicotinamide (Macklin, 99%) was added to 2 mol L⁻¹ (2 M) ZnSO₄ (Aladdin, 99.995%) electrolyte. For I₂@C preparation: 1.0 g I₂ (Aladdin, 99.99%) and 0.1 g activated carbon (~1800 m² g⁻¹, 1.0-1.2 cm³ g⁻¹, Nanjing XFNANO Materials Tech Co., Ltd) were loaded into a sealed glass bottle, then heated at 120°C for 2 h. After cooling down to room temperature, the activated carbon powders were taken out and kept at 100°C for 2 h to remove the redundant iodine. The iodine content was about 67%.

2. Material characterization

X-ray diffraction (XRD) patterns were recorded on a Rigaku D/MAX-2550-PC X-ray diffractometer with Cu K α radiation ($\lambda = 0.154$ nm). The morphology and structure of the samples were characterized using a scanning electron microscope (SEM, SU8010, HITACHI). The pH value was measured by Mettler Toledo FE28. Fourier transform infrared (FTIR) spectrum was recorded by an FTIR spectrometer (Nicolet 6700). In-situ optical microscope images were obtained from a ZW-C200 optical microscope. The ion conductivity of different electrolytes was collected through a conductivity meter (Shanghai Yueping Scientific Instrument Co., Ltd., DDS-11A). X-ray photoelectron spectroscopy (XPS) analysis was performed on Thermo Scientific K-Alpha+, operating with an Al K α radiation source and an ultra-high vacuum. Raman spectra were collected on a Renishaw inVia using a laser with an excitation wavelength of 532 nm.

3. DFT calculation

DFT calculations were performed using the PBE approximation method [1] of the generalized gradient approximation functional (GGA) using the ab initio VASP package [2-3]. The plane wave pseudopotential (PAW) [4-5] is chosen to describe the interaction between atomic nuclei and electrons, and the cutoff energy of the plane wave basis set is 450 eV. Van der Waals interactions are considered by using Grimme's DFT-D3 method [6]. In the geometry optimization, the energy and force convergence criteria for the self-consistent field are set to 1×10^{-5} eV and 0.02 eV \AA^{-1} , respectively. In the relaxation process, the Gamma grid K point selected for the reciprocal space Brillouin zone is $2 \times 2 \times 1$. Set the vacuum height to 20 \AA to remove the effect of periodicity. Simultaneously, spin polarization calculations were performed. The adsorption energy for the NTA molecule is calculated as:

$$E_{ads} = E_{NTA@Zn} - E_{NTA} - E_{Zn}$$

Where $E_{NTA@Zn}$, E_{NTA} , and E_{Zn} represent the total energy of adsorbed NTA on Zn, the energy of the NTA molecule, and the energy of Zn, respectively.

4. Electrochemical measurements

For the cyclic voltammetry (CV) test of zinc deposition, titanium foil, saturated calomel electrode (SCE), and platinum wire were used as deposition substrate, reference electrode, and counter electrode, respectively. The applied voltage for the chronoamperometry (CA) test was -130 mV vs. OCV. For corrosion current measurement, zinc foil, platinum wire, and SCE were used as working electrode, counter electrode, and reference electrode, respectively, and the test voltage range was -1.3 ~ -0.7 V vs. SCE; the corrosion current was calculated from Tafel fit system in electrochemical workstation. The I₂@C cathode was obtained by mixing 80 wt.% I₂@C composites, 10 wt.%

polytetrafluoroethylene (PTFE, 10 wt.% in water), and 10 wt.% Super P together, then rolling the mixture into a thin film and cutting into a circular flake with a diameter of 12 mm, finally pressing on the Ti mesh current collector. After drying, the areal mass loading of I₂@C in the electrode is about 1.0-3.0 mg cm⁻². The current densities and specific capacities were all normalized to the weight of iodine. The electrochemical tests of Zn-Zn symmetric batteries, Cu-Zn asymmetric batteries, and Zn-I₂ full batteries were all conducted in CR2025-type coin cells assembled in the air, where the glass fiber membrane was used as the separator. LAND battery testers (CT3001A) were used to conduct the constant current discharge/charge measurements of all cells. CV, CA, and electrochemical impedance spectroscopy (EIS) were all conducted on a CHI660E electrochemical workstation. EIS was measured between 0.01 and 10⁵ Hz with an excitation voltage of 5 mV

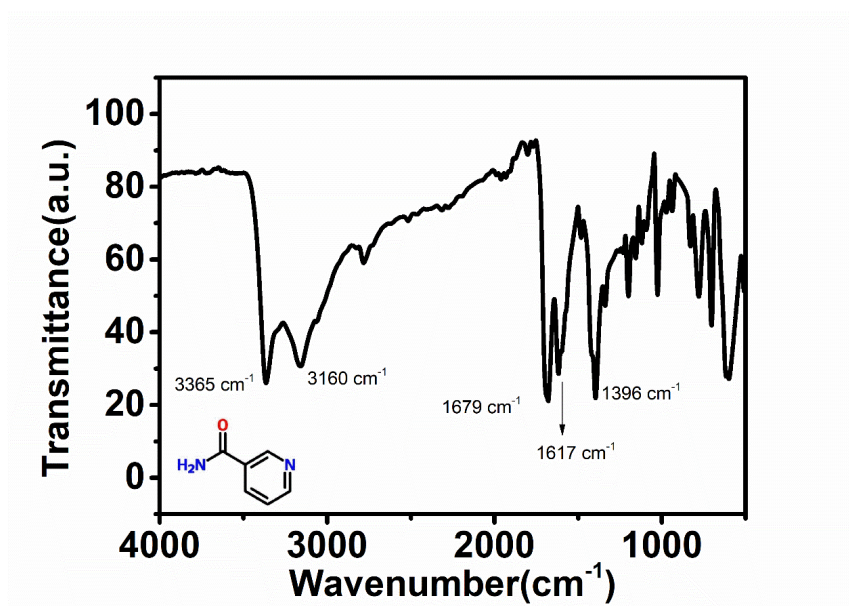


Figure S1. The FTIR spectrum and molecular structure of NTA.

Two sharp peaks at 3365 and 3160 cm⁻¹ are antisymmetric and symmetric stretching vibrations of the N-H bond, respectively. 1679 cm⁻¹ is assigned to C=O stretching vibration, 1617 cm⁻¹ belongs to N-H bending vibration, 1396 cm⁻¹ is stretching vibration of the C-N bond, and the peaks ranging from 700 to 900 cm⁻¹ are out-of-plane bending vibrations of C-H bond on the aromatic ring.

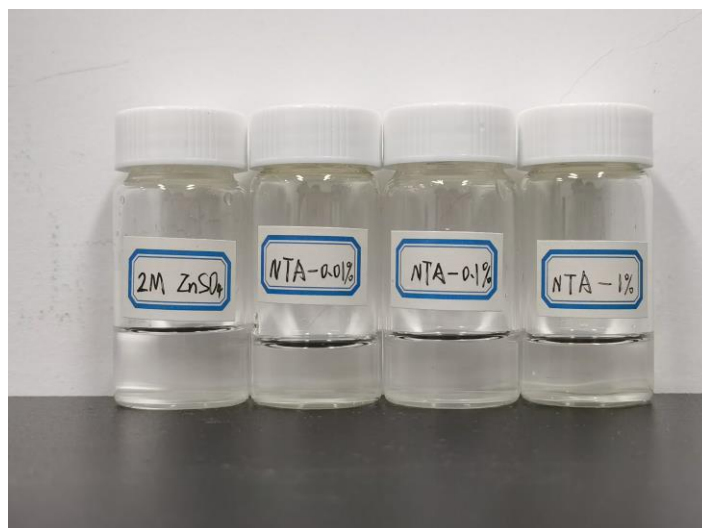


Figure S2. Photographs of four electrolytes studied in this work. There are no obvious differences in the appearance of the four electrolytes, including color and transparency.

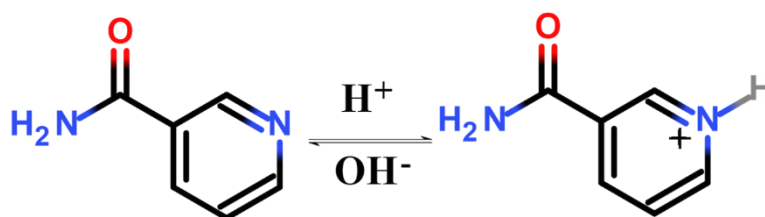


Figure S3. NTA molecule can combine with H^+ to improve the electrolyte pH value of 2 M ZnSO_4 .

Table S1. The pH values of four electrolytes.

Group	1	2	3	Average
2 M ZnSO_4	3.79	3.80	3.81	3.80
NTA-0.01%	3.85	3.85	3.84	3.85
NTA-0.1%	4.12	4.10	4.11	4.11
NTA-1%	4.44	4.43	4.44	4.44

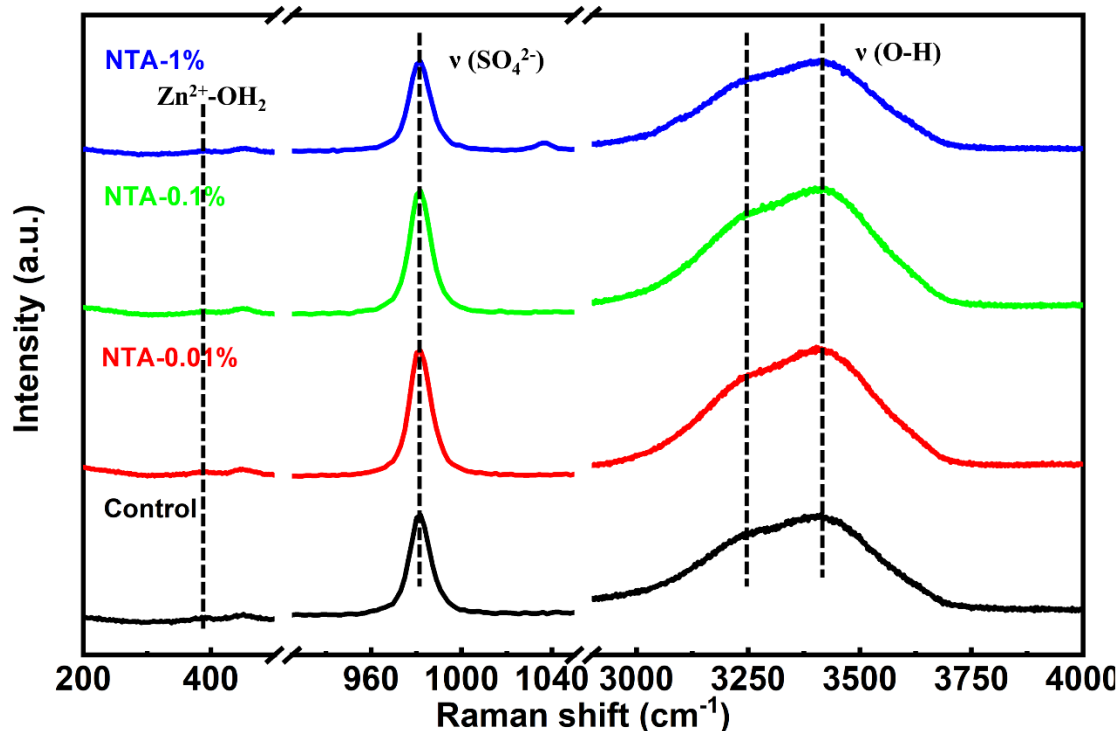


Figure S4. Raman spectra of the different electrolytes.

There were no observable changes or shifts in the characteristic peaks of $\text{Zn}^{2+}\text{-OH}_2$, SO_4^{2-} , and O-H in both pure ZnSO_4 electrolyte and NTA-containing electrolytes. Hence, there is no direct evidence supporting the notion that NTA molecules affect the solvation sheaths of Zn^{2+} in the above NTA-containing electrolytes. However, the ionic conductivity of NTA-based electrolytes decreases compared to pure 2M ZnSO_4 , indirectly suggesting that NTA molecules may coordinate with Zn^{2+} and slow down their migration and diffusion rate. The low dosage of NTA used in this study may explain the lack of a significant effect on the Zn^{2+} solvation shell. NTA exhibits high solubility in water, with a solubility of 100 g per 100 mL of water. However, the NTA dosage utilized in this study is relatively low. To illustrate this, consider the weight of 25 mL of a 2M ZnSO_4 solution, which amounts to 32.3 g. Among this weight, the solute ZnSO_4 accounts for 8.05 g, while the remaining 24.25 g corresponds to the weight of water. On the other hand, in the case of the NTA-1% electrolyte, 0.323 g of NTA is added, signifying that 1.33 g ($0.323 \times 100 / 24.25$) of NTA is soluble in a 100 g quantity of water.

Table S2. The ionic conductivity of four electrolytes.

Group	①	②	③	Average (mS/cm)
2M ZnSO_4	36.0	36.4	36.2	36.2
NTA-0.01%	35.8	36.2	36.2	36.1
NTA-0.1%	34.8	34.8	34.7	34.8
NTA-1%	33.1	32.5	32.7	32.8

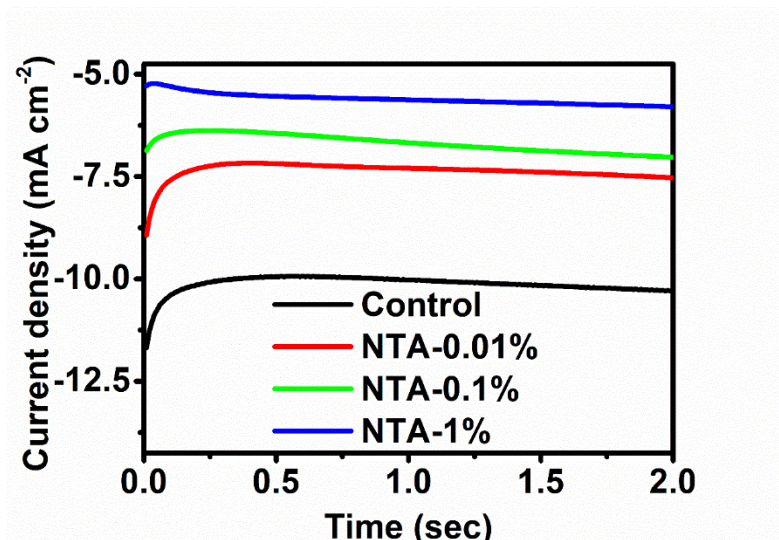


Figure S5. The initial two seconds of the CA test under an overpotential of -130 mV vs. OCV

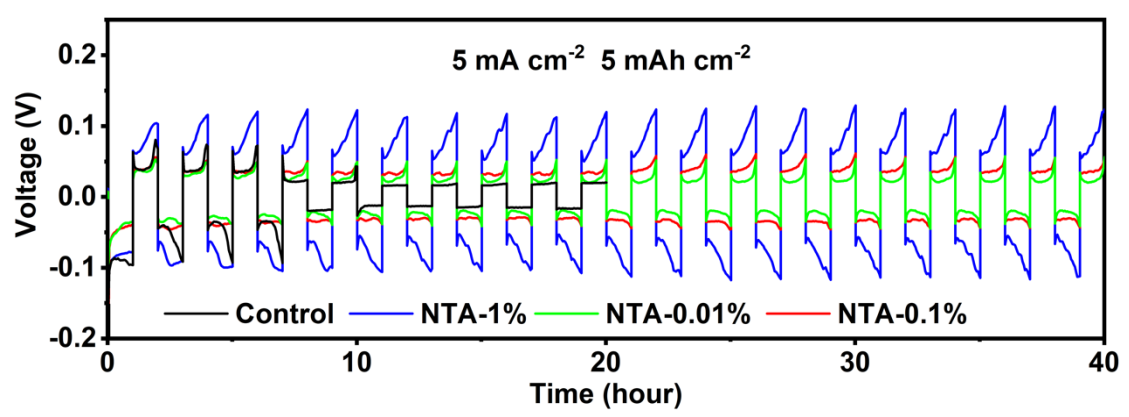


Figure S6. Enlarged view of Figure 2a

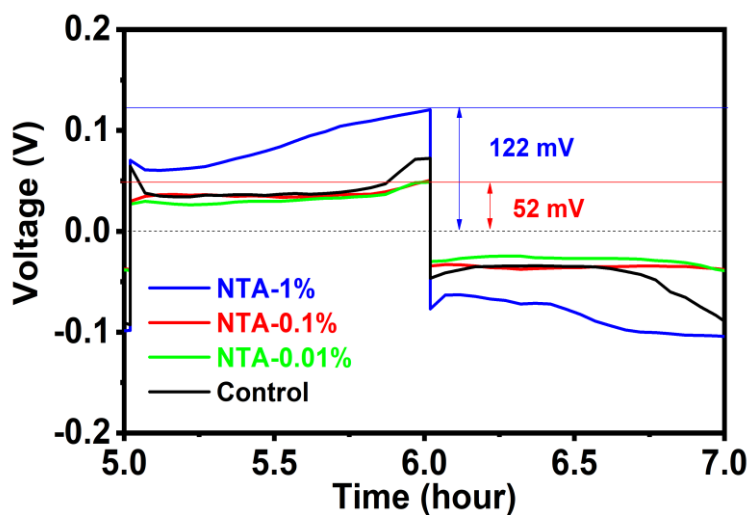


Figure S7. High-resolution voltage profiles in different electrolytes from 5 to 7 h. The overpotential of NTA-1% (122 mV) at 6 h is about 70 mV higher than NTA-0.1% (52 mV).

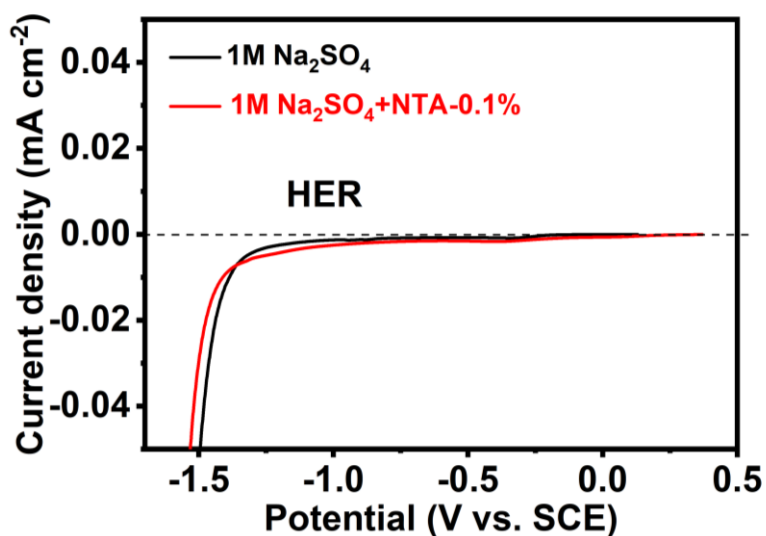


Figure S8. Linear sweep voltammetry curves in 1 M Na_2SO_4 and 1 M Na_2SO_4 +NTA-0.1% electrolyte at a scan rate of 2 mV s^{-1} . SCE, Pt wire, and glassy carbon electrode were used as the reference electrode, the counter electrode, and the working electrode, respectively. Because it is difficult to observe the HER process in the ZnSO_4 electrolyte at similar potentials of zinc deposition, Na_2SO_4 solutions were used to replace ZnSO_4 to eliminate the influence of the Zn deposition on HER.

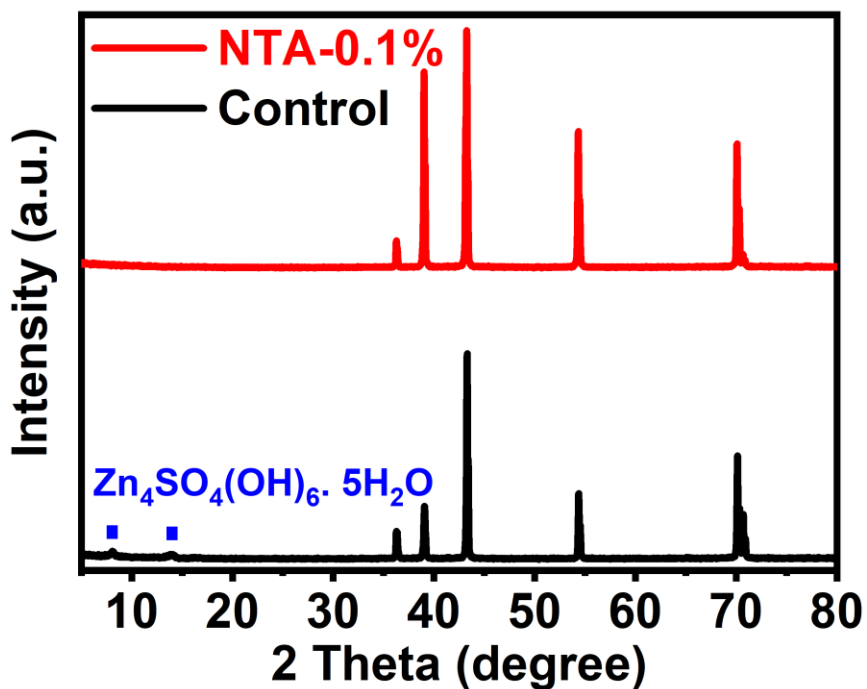


Figure S9. XRD patterns of zinc foils immersed in different electrolytes for a week. Zinc foils were immersed in pure 2 M ZnSO₄ electrolyte and NTA-0.1% for a week and then applied to the XRD test. Both two groups have strong peaks located at 36°, 39°, 42°, 54°, and 70°, which are attributed to (002), (100), (101), (102), and (103) crystallographic planes of metal zinc, respectively.

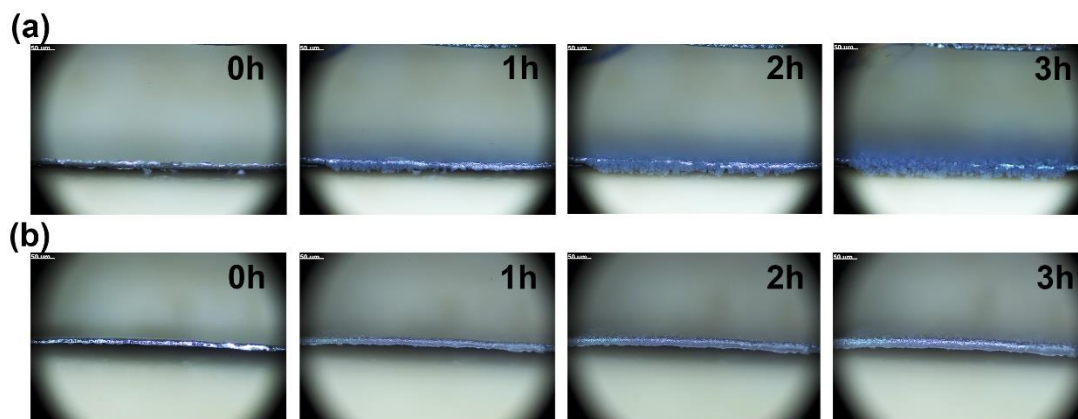


Figure S10. In-situ optical microscope observation of the cross-section of zinc foils was undertaken to intuitively view the zinc deposition process at 5 mA cm⁻² in (a) pure 2M ZnSO₄ electrolyte and (b) NTA-0.1% electrolyte.

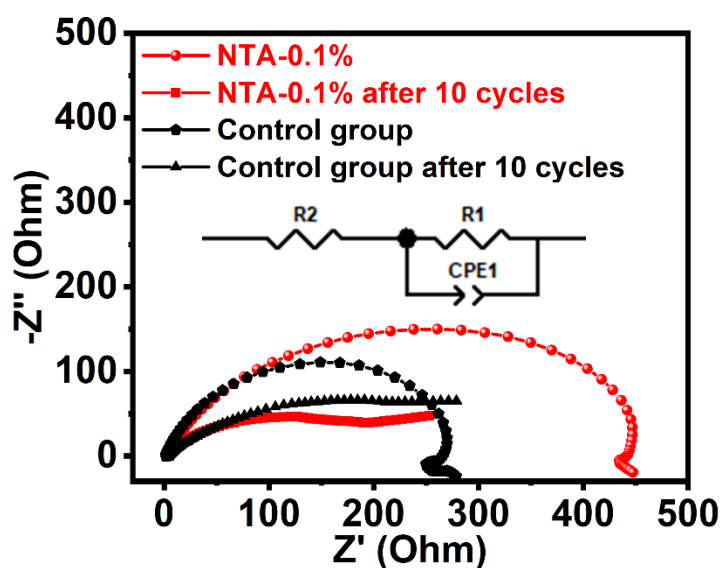


Figure S11. The impedance spectra of Zn-Zn symmetric batteries before and after 10 cycles (1 mA cm^{-2} and 1 mAh cm^{-2}) in two electrolytes. The inset is the equivalent circuit model.

Under static conditions, the presence of NTA molecules on the surface of the zinc foils resulted in an increased charge transfer resistance ($489.6 \text{ vs. } 294.8 \Omega$), which aligns with the observed NOP and voltage polarization. After 10 cycles, the R_{ct} values for both groups significantly decreased, indicating battery system activation. However, the R_{ct} value for the NTA-0.1% group was much smaller than that of the control group ($201.2 \text{ vs. } 291.2 \Omega$), which could be attributed to the formation of $\text{Zn}_4(\text{OH})_6\text{SO}_4 \cdot x\text{H}_2\text{O}$ with poor electronic conductivity (control group).

Table S3. The corresponding fitting results of the EIS of the Zn||Zn symmetric batteries

	Control group	Control group after 10 cycles	NTA-0.1%	NTA-0.1% after 10 cycles
$R_1 (R_{ct})$	294.8	291.2	489.6	201.2
$R_2 (R_{\Omega})$	2.367	1.929	0.401	1.624

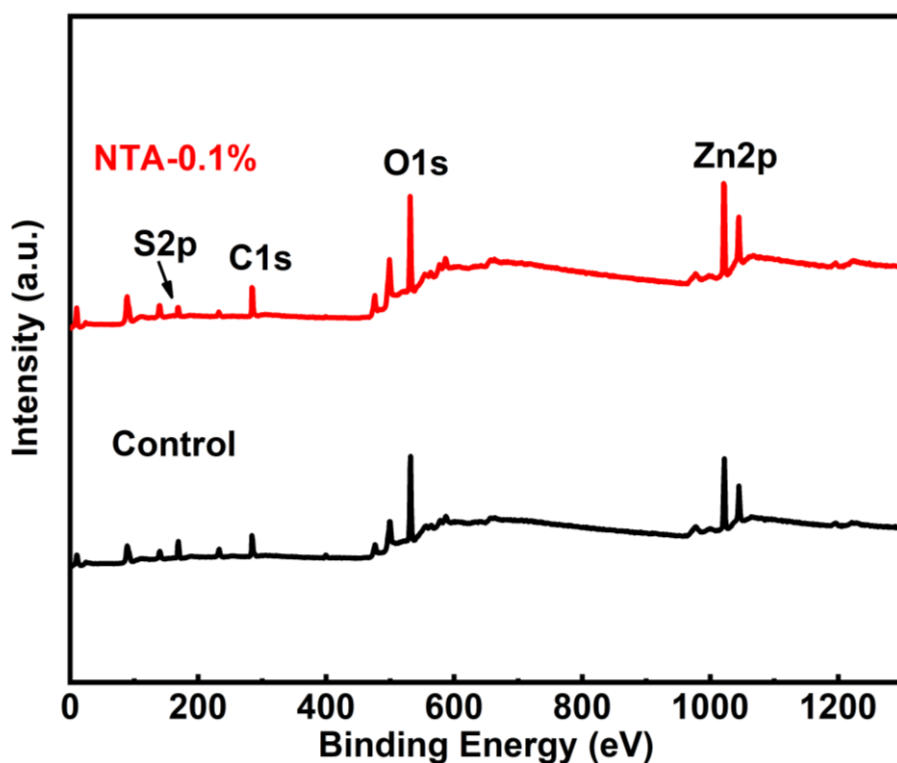


Figure S12. XPS full-survey spectra of zinc anodes after 10 cycles in two electrolytes.

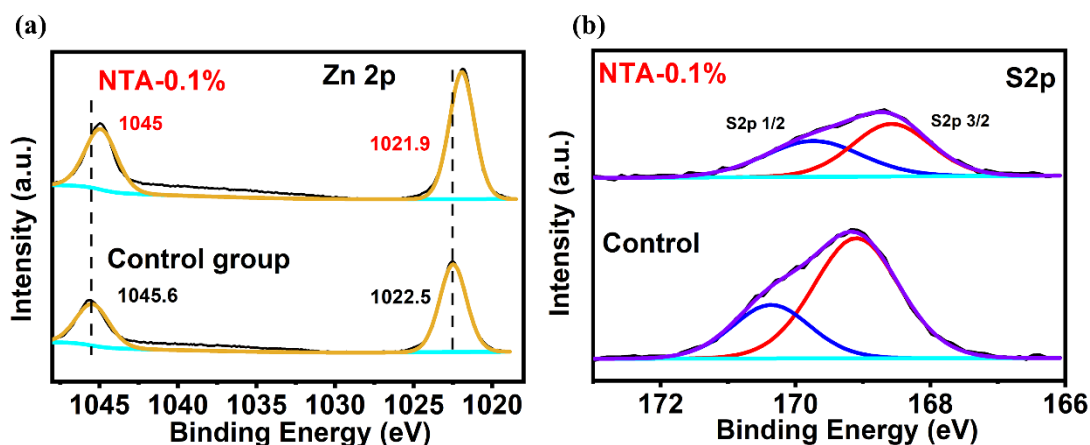


Figure S13. The high-resolution XPS of zinc anodes after 10 cycles in two electrolytes: (a) Zn2p and (b) S2p.

The binding energies of Zn2p in the control group were measured to be 1045.6 eV (2p_{1/2}) and 1022.5 eV (2p_{3/2}), higher than NTA-0.1% with binding energies of 1045 and 1021.9 eV (atomic Zn), indicating the presence of Zn²⁺ (ZnSO₄, ZnO, Zn(OH)₂, or ZHS). This suggests that the substances on the zinc anode surface in the control group are mainly side reaction products, whereas in the NTA-0.1% group, they are primarily zinc. The high-resolution XPS results of S2p support the above inference, with the intensity of SO₄²⁻ (originating from ZnSO₄ and ZHS) in the control group being much higher than that in NTA-0.1%. Therefore, the XPS results confirm the suppressive effect of NTA additives on side reactions.

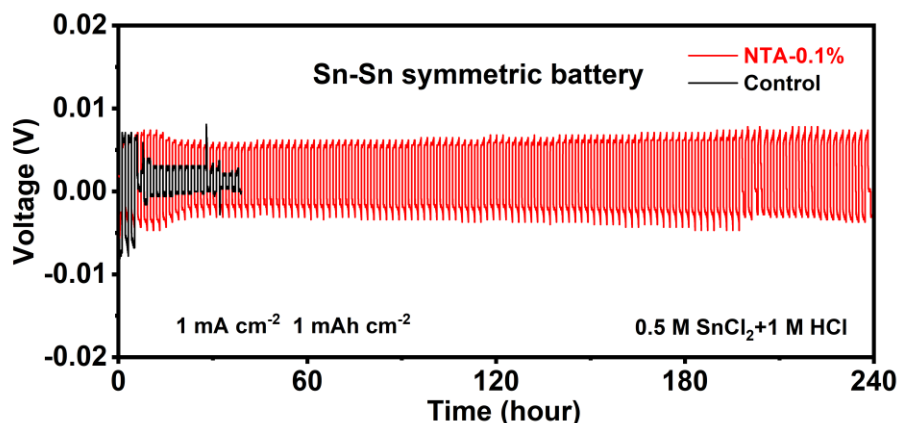


Figure S14. The voltage-time curves of Sn-Sn symmetric batteries with/without NTA additives. To confirm the applicability of NTA additives to other material systems, the deposition of Sn^{2+} was chosen for testing. Recently, the Sn metal anode for aqueous batteries was reported [7-8], which illustrates the value of Sn deposition in the battery field. So, 0.5 M SnCl_2 +1 M HCl was used as the electrolyte according to Ref. 7, and the deposition stability of Sn-Sn symmetric batteries was investigated with/without NTA additives under 1 mA cm^{-2} and 1 mAh cm^{-2} . In Figure S14, the control group exhibited a sudden and irreversible voltage drop after cycling for 8 h. In contrast, the lifespan of NTA-0.1% was significantly prolonged, allowing the symmetric battery to operate smoothly within 240 hours without apparent voltage fluctuations. Hence, the NTA additives also can regulate the deposition performance of Sn^{2+} .

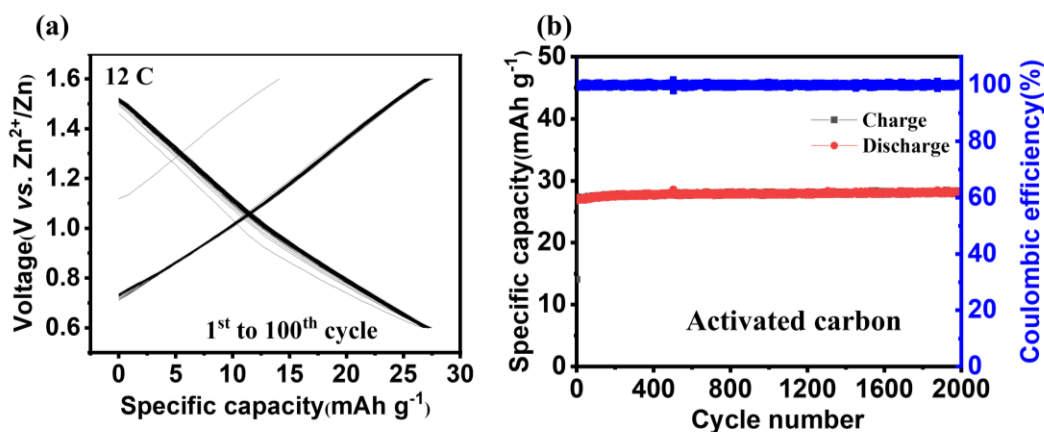


Figure S15. The electrochemical performance of activated carbon: (a) Charge-discharge curves, (b) long-term cycling stability.

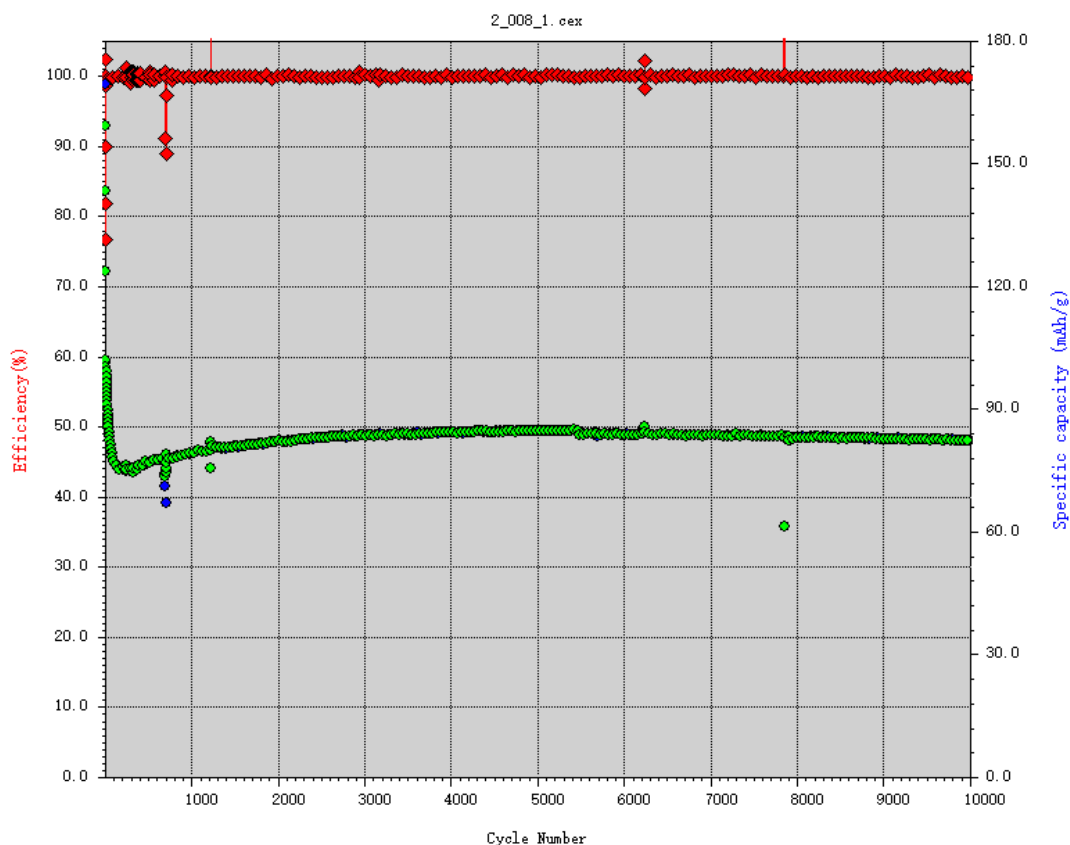


Figure S16. The screenshot of the long cycling stability of the aqueous zinc iodine battery with NTA-0.1%.

All full batteries were activated at 1 C (211 mA g^{-1}) for 3 cycles and tested at 12 C for the subsequent cycles. Due to the limited adsorption effect of active carbon, a rapid capacity decay caused by the dissolution of iodine species is observed in both two electrolytes; however, they are rather stable in the follow-up cycles. The first discharge capacities of the control group and NTA-0.1% at 1C are 207 and 197.1 mAh g^{-1} with ICEs of 81.9% and 79.5%, respectively. The 4th cycle capacity of NTA-0.1, corresponding to the first cycle at 12 C, is 98.2 mAh g^{-1} and the capacity at the 10000th cycle is 82.3 mAh g^{-1} . Therefore, the capacity retention is 83.7% according to the data.

Table S4. Comparison of the reported electrolyte additives for zinc anode.

Electrolyte Additives	Symmetric Batteries			Asymmetric Batteries (Average CE)	Full batteries		Ref.
	Long Lifespan	Harsh Condition	Voltage hysteresis		Cathode and Electrolyte	Performance (Capacity retention)	
Nicotinamide (NTA)	1 mA cm ⁻² and 1 mAh cm ⁻² for 500 h;	5 mA cm ⁻² and 5 mAh cm ⁻² for 200 h;	52 mV at 5 mA cm ⁻²	99.0% at 1 mA cm ⁻² and 1 mAh cm ⁻²	I ₂ @AC 2M ZnSO ₄ +NTA-0.1%	83.7% after 10000 cycles	This work
Arginine (Arg)	1 mA cm ⁻² and 1 mAh cm ⁻² for 2950 h;	10 mA cm ⁻² and 4 mAh cm ⁻² for 900 h;	~60 mV at 5 mA cm ⁻²	98.3% at 1 mA cm ⁻² and 1 mAh cm ⁻²	α-MnO ₂ 3M ZnSO ₄ + 0.1 M Arg	83.0% after 200 cycles	[9]
2-Bis (2-hydroxyethyl) amino-2-(hydroxymethyl)-1,3-propanediol (BIS-TRIS)	1 mA cm ⁻² and 1 mAh cm ⁻² for 1200 h;	5 mA cm ⁻² and 5 mAh cm ⁻² for 600 h;	~100 mV at 5 mA cm ⁻²	98.5% at 1 mA cm ⁻² and 1 mAh cm ⁻²	MnO ₂ 2M ZnSO ₄ +0.1 M BIS-TRIS	neglected capacity decay after 600 cycles	[10]
Urea	1 mA cm ⁻² and 1 mAh cm ⁻² for 700 h	none	~30 mV at 1 mA cm ⁻²	none	Na _{0.1} MnO ₂ 0.5H ₂ O 1M ZnSO ₄ +3 M urea	Stable for 5000 cycles	[11]
Saccharin (Sac)	10 mA cm ⁻² and 10 mAh cm ⁻² for 550 h	40 mA cm ⁻² and 10 mAh cm ⁻² for 220 h;	~75 mV at 10 mA cm ⁻²	99.6% at 10 mA cm ⁻² and 10 mAh cm ⁻²	MnO ₂ 2M ZnSO ₄ +0.5 g L ⁻¹ Sac+0.1M MnSO ₄	Stable for 7500 cycles	[12]
Glucose	1 mA cm ⁻² and 1 mAh cm ⁻² for 2000 h	5 mA cm ⁻² and 5 mAh cm ⁻² for 270 h;	~60 mV at 5 mA cm ⁻²	97.2% at 1 mA cm ⁻² and 0.5 mAh cm ⁻²	MnO ₂ 1 M ZnSO ₄ + 10 mM glucose	~80% after 1000 cycles	[13]
Ethylene diamine tetraacetic acid tetrasodium salt (Na ₄ EDTA)	2 mA cm ⁻² and 2 mAh cm ⁻² for 450 h	5 mA cm ⁻² and 2 mAh cm ⁻² for 2000	~50 mV at 2 mA cm ⁻²	99.5% at 2 mA cm ⁻² and 1 mAh cm ⁻²	VO ₂ 1M ZnSO ₄ +0.075M	>86% after 2000 cycles	[14]

		h;			Na ₄ EDTA		
α -cyclodextrin (α -CD)	1 mA cm ⁻² and 1 mAh cm ⁻² for 8000 h	10 mA cm ⁻² and 10 mAh cm ⁻² for 570 h;	~50 mV at 1 mA cm ⁻²	99.5% at 2 mA cm ⁻² and 0.5 mAh cm ⁻²	MnO ₂ 2M ZnSO ₄ +0.01 α -CD +0.2M MnSO ₄	>79.9% after 600 cycles	[15]
Dextran	10 mA cm ⁻² and 10 mAh cm ⁻² for 800 h	50 mA cm ⁻² and 10 mAh cm ⁻² for 55 h;	~130 mV at 10 mA cm ⁻²	99.97% at 5 mA cm ⁻² and 1 mAh cm ⁻²	V ₂ O ₅ 1 M Zn(CF ₃ SO ₃) ₂ +50 mg mL ⁻¹ Dextran	82.5% after 600 cycles	[16]

We have compiled a table comparing our work to other electrolyte additives that have been reported in high-impact factor (IF) journals. However, we acknowledge that there is a noticeable disparity between our work and those remarkable studies, specifically in terms of the cycle stability of the zinc anode. This difference could be attributed to the depth of discharge (DOD) of the zinc foil utilized in our research. In our work, we used a zinc foil with a thickness of 0.03 mm, resulting in an areal capacity of 17.55 mAh cm⁻². During the testing of the symmetric battery at 5 mAh cm⁻², the DOD reached approximately 28.5%, which surpasses the DOD values reported in the majority of previous studies. Nevertheless, it is worth noting that our work demonstrates competitive performance in voltage hysteresis, average Coulombic efficiency (CE), and cycling stability when compared to those exceptional studies.

Reference:

- [1] PERDEW J P, BURKE K, ERNZERHOF M. Generalized Gradient Approximation Made Simple[J]. Physical Review Letters, 1996, 77(18):3865-3868.
- [2] KRESSE G, FURTHMÜLLER J. Efficiency of Ab-Initio Total Energy Calculations for Metals and Semiconductors Using a Plane-Wave Basis Set[J]. Computational Materials Science, 1996, 6(1):15-50.
- [3] KRESSE G, FURTHMÜLLER J. Efficient Iterative Schemes for Ab Initio Total Energy Calculations Using a Plane-Wave Basis Set[J]. Physical Review B, 1996, 54(16):11169-11186.
- [4] KRESSE G, JOUBERT D. From Ultrasoft Pseudopotentials to the Projector Augmented-Wave Method[J]. Physical Review B, 1999, 59(3):1758-1775.
- [5] BLÖCHL P E. Projector Augmented-Wave Method[J]. Physical Review B, 1994, 50(24):17953-17979.
- [6] GRIMME S, ANTONY J, EHRLICH S, et al. A Consistent and Accurate Ab Initio Parametrization of Density Functional Dispersion Correction (DFT-D) for the 94 Elements H-Pu[J]. The Journal of Chemical Physics, 2010, 132(15):154104
- [7] Zhang H., Xu D., Yang F., Xie J., Liu Q., Liu D., Zhang M., Lu X., Meng Y., A high-capacity Sn metal anode for aqueous acidic batteries. Joule, 2023, 92: 971-978
- [8] Zhou W., Ding S., Zhao D., Chao D., An energetic Sn metal aqueous battery. Joule, 2023, 7: 1104-1107
- [9] Lu H, Zhang X, Luo M, Cao K, Lu Y, Xu B, Pan H, Tao K, Jiang Y. Amino acid-induced interface charge engineering enables highly reversible Zn anode. Advanced Functional Materials, 2021, 31: 2103514.

- [10] Luo M, Wang C, Lu H, Lu Y, Xu B, Sun W, Pan H, Yan M, Jiang Y. Dendrite-free zinc anode enabled by zinc-chelating chemistry. *Energy Storage Materials*, 2021, 41: 515-521.
- [11] Hou Z, Dong M, Xiong Y, Zhang X, Ao H, Liu M, Zhu Y, Qian Y. A high-energy and long-life aqueous Zn/birnessite battery via reversible water and Zn^{2+} coinsertion. *Small*, 2020, 16(26): 2001228.
- [12] Huang C, Zhao X, Liu S, et al. Stabilizing zinc anodes by regulating the electrical double layer with saccharin anions. *Advanced materials*, 2021, 33(38): 2100445.
- [13] Sun P, Ma L, Zhou W, et al. Simultaneous regulation on solvation shell and electrode interface for dendrite-free Zn ion batteries achieved by a low-cost glucose additive. *Angewandte Chemie*, 2021, 133(33): 18395-18403.
- [14] Zhang S J, Hao J, Luo D, et al. Dual-function electrolyte additive for highly reversible Zn anode. *Advanced Energy Materials*, 2021, 11(37): 2102010.
- [15] Yang J, Yin B, Zhang S, et al. Macromolecules Promoting Robust Zinc Anode by Synergistic Coordination Effect and Charge Redistribution. *Small*, 2023: 2304913.
- [16] Li J, Guo Z, Wu J, et al. Dextran: A Multifunctional and Universal Electrolyte Additive for Aqueous Zn Ion Batteries. *Advanced Energy Materials*, 2023: 2301743.